Elimination of X-Ray Diffraction through Stimulated X-Ray Transmission

B. Wu,[1] T. Wang,[2] C. E. Graves,[1] D. Zhu,[3] W. F. Schlotter,[3] J. Turner,[3]
O. Hellwig,[4] Z. Chen,[5] H. A. Dürr,[3] A. Scherz,[6, *] and J. Stöhr[3, †]

[1]*SLAC National Accelerator Laboratory and Dept. of Applied Physics, Stanford, USA*
[2]*SLAC National Accelerator Laboratory and Dept. Mat. Science and Engineering, Stanford, USA*
[3]*SLAC National Accelerator Laboratory, 2575 Sand Hill Road, Menlo Park, CA 94025, USA*
[4]*HGST, a Western Digital Company, 3403 Yerba Buena Road, San Jose, CA 95135, USA*
[5]*SLAC National Accelerator Laboratory, and Dept. of Physics, Stanford, USA*
[6]*European XFEL GmbH, Albert-Einstein-Ring 19, 22761 Hamburg, Germany*

X-ray diffractive imaging with laterally coherent x-ray free electron laser (X-FEL) pulses is increasingly utilized to obtain ultrafast snapshots of matter. Here we report the amazing disappearance of single-shot charge and magnetic diffraction patterns recorded with resonantly tuned, narrow bandwidth X-FEL pulses. Our experimental results reveal the exquisite sensitivity of single-shot charge and magnetic diffraction patterns of a magnetic film to the onset of field-induced stimulated elastic x-ray forward scattering. The loss in diffraction contrast, measured over three orders of magnitude in intensity, is in remarkable quantitative agreement with a recent theory that is extended to include diffraction.

Over the last decade, the technique of coherent x-ray diffractive imaging has been developed to understand states of matter that are neither crystalline nor stationary and are often confined to nanometer dimensions [? ? ? ? ? ? ? ? ?]. The technique can also circumvent structural x-ray damage by use of femtosecond pulses from x-ray free electron lasers (X-FELs) that are faster than atomic motion [? ?]. Diffraction imaging of *atomic structure* with hard x-rays (∼10 keV) typically utilizes non-resonant *Thomson scattering* arising from the collective elastic x-ray response of the atomic electron clouds. Soft x-ray (∼1 keV) imaging of *nanoscale domains* usually employs *resonant scattering* based on specific core-to-valence transitions, which offer enhanced cross sections, and elemental, chemical and magnetic specificity.

Single shot diffractive imaging necessarily requires high intensity X-FEL pulses. By now, various high field effects induced by such pulses have been reported, such as multiple ionization [?], self amplified spontaneous x-ray emission [?] and stimulated x-ray Raman scattering [?]. Recently, it has been predicted theoretically that it is possible to drive resonant core-to-valence transitions to induce x-ray transparency [?]. Here we provide experimental proof of the existence of stimulated elastic scattering into the forward direction of the incident beam by linking it to the loss of the out-of-beam diffracted intensity.

Using a coherent imaging geometry and 50 fs X-FEL pulses from the Linac Coherent Light Source (LCLS), monochromatized and tuned to the Co L$_3$ resonance at 778 eV, we observe the gradual disappearance of magnetic diffraction contrast and the reduction of charge diffraction contrast above an intensity of 10 mJ/cm^2/pulse, well below the multiple ionization threshold. Our experimental results, covering nearly three orders of magnitude of incident intensities, are in quantitative agreement with the theory of Ref. [?], ex-

tended to include diffraction, without adjustment of parameters.

Experiments were performed at the soft x-ray (SXR) station of LCLS using *linearly polarized* x-rays in the geometry illustrated in Fig. **??**. The incident self ampli-
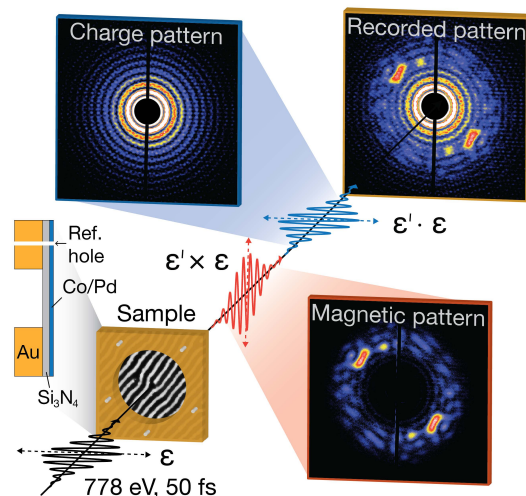

FIG. 1: Experimental geometry. Linear polarized x-ray pulses of 50 fs temporal width and monochromatized to an energy of 778±0.1 eV, were focussed to a spot size of 10μm FWHM onto a 1.45μm diameter aperture in front of a Co/Pd multilayer sample. The shown diffraction pattern of a typical Co/Pd worm domain sample was recorded with a CCD detector placed 490 mm behind the sample by use of low intensity pulses, tuned to the Co L$_3$ resonance at 778 eV. Owing to the orthogonal polarization of charge and spin scattering, the composite diffraction pattern could be decomposed, as shown, by subtracting the scaled charge-only Airy pattern recorded at 765 eV, where resonant magnetic diffraction is absent. The centrally transmitted intensity was blocked by a beam stop in front of the detector.

fied spontaneous emission (SASE) pulses of about 50 fs full width at half maximum (FWHM) were sent through a grating monochromator, resulting in a photon energy of 778±0.1 eV as discussed below, and focused onto the sample by a Kirkpatrick-Baez optic to a spot size of $10 \mu m$ FWHM. The Co/Pd multilayer sample, containing magnetic worm domains with perpendicular magnetization directions [? ?] was illuminated through a $1.45\,\mu m$ diameter circular aperture in a Au film. Five reference holes of 100 nm diameter, arranged in a pentagon, were ion beam drilled through the entire sample/mask to create a reference pattern [?]. The centrally transmitted beam was blocked by a beam stop in front of the detector.

The transmission of linear polarized x-rays through a magnetic sample, which consists of domains with opposite magnetization directions along the x-ray propagation direction, is best described by considering the transmission of the orthogonal left and right circular components. The transmitted *intensity*, which is determined by the *sum* of the transmitted right and left circular field amplitudes, is not affected by the magnetic structure. The transmitted intensity in the forward direction (momentum transfer $\boldsymbol{q} = 0$) is therefore only due to the charge response. Absorption by the charge density causes a uniform attenuation of the Airy ring diffraction pattern created by the circular aperture before the sample. A magnetic effect arises only from a change in the *phase* of the transmitted field. When viewed in a linear polarization basis, the phase change creates a (weak) field component that is rotated by ±90°, giving rise to the magneto-optical Faraday effect [? ?]. Oppositely magnetized domains give rise to opposite 90° rotations, and the relative 180° phase difference then leads to an interference pattern at finite momentum transfer $\boldsymbol{q}$. We distinguish this pure magnetic diffraction pattern and its intensity from the Airy diffraction pattern caused by the aperture before the sample whose intensity is determined by charge-based absorption in the sample with preservation of the incident polarization.

Diffraction patterns were recorded by a CCD camera, placed 490 mm downstream of the sample. For each sample, a baseline diffraction pattern was recorded with 360 x-ray pulses of low fluence ($\sim 10^{10}$ W/cm^2) at two energies, on-resonance at 778 eV, and at 765 eV, where magnetic scattering is absent and only the pure Airy ring pattern is observed. The gas attenuation was then reduced, and a single shot high intensity diffraction pattern was recorded at 778 eV with fluences ranging between $10^{11} - 10^{13}$ W/cm^2. The energy per pulse was measured with two transmission gas detectors. We also calibrated the response of the CCD detector which operated in single photon counting mode. This allowed an independent shot-to-shot intensity measurement through the cross-correlation intensity between the five reference holes [?]. We estimate error bars of $<30\%$ for the absolute and $<5\%$ for the relative intensities.
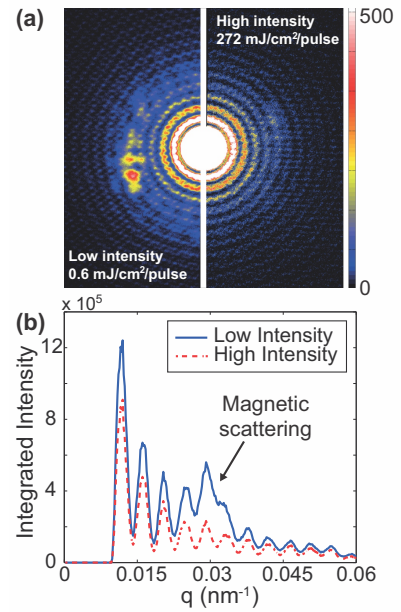

FIG. 2: (a) Diffraction patterns recorded with low (left half) and high (right half) incident intensity for a magnetic worm domain sample. (b) Azimuthally integrated diffraction contrast as a function of momentum transfer (q) for the two patterns in (a). The magnetic signal is located around $q = 0.03\,\text{nm}^{-1}$

Characteristic low and high intensity diffraction patterns are shown in Fig. **??** (a). We only show half of the patterns since they exhibit inversion symmetry about the center. In the low-intensity (0.6 mJ/cm^2/pulse) reference pattern, the magnetic speckles are clearly visible and distinct from the Airy rings, which originate from the circular aperture and are attenuated by the film. The corresponding high-intensity (272 mJ/cm^2/pulse) diffraction pattern reveals a dramatic decrease of the magnetic diffraction intensity. In Fig. **??** (b) we show the intensity of the patterns in (a), azimuthally integrated around the beam direction, as a function of momentum transfer q. They reveal that in addition to the magnetic diffraction signal around $q = 0.03$ nm^{-1}, the intensity of all Airy rings is also reduced by the same relative amount at high incident intensity. The intensity of the central Airy pattern was blocked by the beamstop and not recorded.

Simulations of the incident pulse structure in the energy and time domain [?], before and after the monochromator, are shown in Fig. **??**. The 50 fs SASE pulses of 778 eV central energy before the monochromator shown in Fig. **??** (a) and (b) consist of many coherent spikes in both the time and energy domain, arising from ordered regions in the x-ray generating electron bunch. The statistical coherence time of these pulses is only about 0.5 fs FWHM [? ?] and the total bandwidth is about 5 eV FWHM. The bandwidth was reduced and the coherence time increased by use of the SXR monochro-
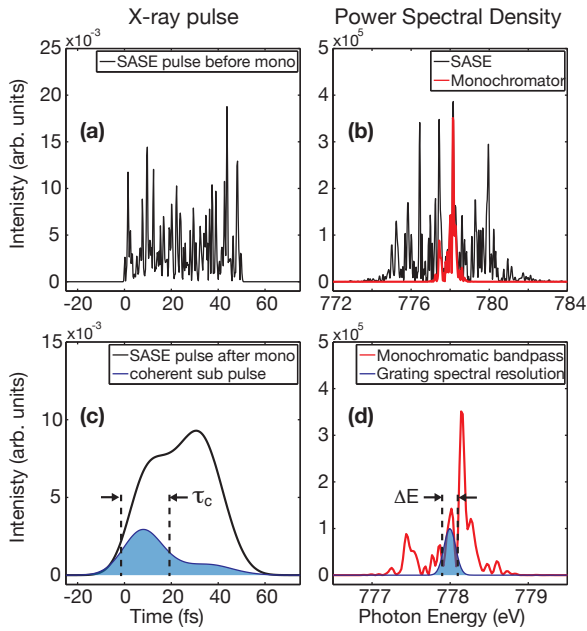
FIG. 3: Fine structure of the SASE pulses of 50 fs duration incident on the grating monochromator in the time (a) and energy domain (b). In (b) the fraction within the monochromator bandpass determined by the exit slit ($\simeq 1$ eV) is shown in red and repeated in (d). The actual spectral resolution $\Delta E = 0.2$ eV (FWHM) is determined by the resolving power of the grating (4000) and the 1.45 μm diameter of the circular Au aperture. It is illustrated by the blue region in (d). The corresponding pulse substructure in the time domain and the effective coherence time τ_C are shown in (c).

mator with a grating line density of 100 lines/mm and a resolving power of 4000 [?]. The nominal resolution of 1 eV FWHM given by the used exit slit width was furthermore reduced to 0.2 eV FWHM by the 1.45 μm diameter apertures before the samples, owing to the fact that they were positioned in the focal plane of the Kirkpatrick-Baez optic that imaged the exit slit onto the sample. As illustrated for a characteristic single shot simulation in Fig. ?? (c) and (d), the resulting temporal pulses consist of two coherent subpulses of $\tau_C \simeq 20$ fs FWHM duration.

The relatively long coherence time of the subpulses allowed us to simulate the non-linear response of the sample by use of the analytical equilibrium expressions of Ref. [?]. They are here extended to analytical expressions describing diffraction. Employing an optical constant formalism which is related to the scattering length description by $\delta = \rho_a \lambda^2 (r_0 Z + f')/2\pi$ and $\beta = \rho_a \lambda^2 f''/2\pi$ [? ?], where r_0 is the Thomson scattering length, Z is the atomic number and ρ_a the atomic number density (90.9 atoms/nm^3 for Co). The polarization ($p = 0, \pm$) dependent Beer-Lambert law for the polarization dependent *transmitted* intensity in the forward direction $\boldsymbol{q} = 0$ then reads [?],

$$I_{\text{trans}}^p = I_0^p \, e^{-2(\beta_0^p + \beta_{\text{NL}}^p)kd} \tag{1}$$

The intensity $I_{\text{trans}}^0 = (I_{\text{trans}}^+ + I_{\text{trans}}^-)/2$ yields the x-ray absorption spectrum (XAS), which is entirely determined by the charge density of the sample. The difference intensity $I_{\text{trans}}^- - I_{\text{trans}}^+$ with $I_0^+ = I_0^-$ is referred to as the x-ray magnetic circular dichroism (XMCD) spectrum [?]. In Eq. (??) the *spontaneous* optical constant β_0^p is given by,

$$\beta_0^p = \frac{\lambda^3 \rho_a \Gamma_x^p}{8\pi^2} \frac{\Gamma/2}{(\hbar\omega - \mathcal{E}_0)^2 + (\Gamma/2)^2} \tag{2}$$

For the Co L$_3$ resonance we have $\lambda = 1.59$ nm and the polarization dependent dipole transition widths are $\Gamma_x^+ = 1.208$ meV, $\Gamma_x^0 = 0.96$ meV, and $\Gamma_x^- = 0.715$ meV, and the core hole life time width is $\Gamma = 430$ meV (see Table 1 in Ref. [?]). The non-linear (NL) contribution β_{NL}^p is given by the equilibrium expression [?],

$$\beta_{\text{NL}}^p = -2\beta_0^p \frac{I_0^p \Gamma_x^p \mathcal{G}_{\text{coh}} \lambda^3/(8\pi^2 c)}{(\hbar\omega - \mathcal{E}_0)^2 + (\Gamma/2)^2 + I_0^p \Gamma_x^p \mathcal{G}_{\text{coh}} \lambda^3/(4\pi^2 c)} \tag{3}$$

Here $\mathcal{G}_{\text{coh}} = N_a \lambda^2/(4\pi A)$ is the enhancement factor for coherent forward scattering by a sample with atomic areal density $N_a/A = \rho_a d$, where d is the sample thickness.

At high incident intensity, Eq. (??) has the limit $\beta_{\text{NL}}^p \rightarrow -\beta_0^p$ and the sample becomes transparent. The polarization dependent optical constants may be redefined in terms of a polarization *independent* charge response, δ, β, and a magnetic response, $\Delta\delta, \Delta\beta$, that depends on the difference in transmission of left and right circular polarization components according to,

$$\delta = \frac{\delta^+ + \delta^-}{2} = \delta_0 + \delta_{\text{NL}}, \quad \beta = \frac{\beta^+ + \beta^-}{2} = \beta_0 + \beta_{\text{NL}} \tag{4}$$

$$\Delta\delta = \frac{\delta^+ - \delta^-}{2} = \Delta\delta_0 + \Delta\delta_{\text{NL}}, \quad \Delta\beta = \frac{\beta^+ - \beta^-}{2} = \Delta\beta_0 + \Delta\beta_{\text{NL}}$$

We also have $(\beta_0^+ + \beta_0^-)/2 = \beta_0^0 = \beta_0$ and similarly for δ.

In the presence of stimulation, the ratio of the stimulated to spontaneous XMCD intensity, is given by,

$$\frac{I_{\text{XMCD}}^{\text{stim}}}{I_{\text{XMCD}}^{\text{spon}}} = \frac{e^{-2(\beta_0 + \beta_{\text{NL}})kd} \sinh[2(\Delta\beta_0 + \Delta\beta_{\text{NL}})kd]}{e^{-2\beta_0 kd} \sinh[2\Delta\beta_0 kd]} \tag{5}$$

The XMCD signal only exists for incident circular polarization ($\Delta\beta \neq 0$) and is confined to the forward direction $\boldsymbol{q} = 0$. It is zero for linear polarization as used here and in any case would have been blocked by the beam stop.

The *diffracted* ($\boldsymbol{q} \neq 0$), Airy and magnetic speckle (which exists even for linear polarization) patterns do not interfere for linear polarization as illustrated in Fig. ??. For an aperture of area $A = \pi R^2$ the Airy pattern at a detector at distance z_0 from the film, in the presence of stimulation is given by,

$$I_{\text{Airy}}^{\text{stim}}(q) = F_{\text{NL}}(q) \underbrace{I_0^0 \frac{A^2}{\lambda^2 z_0^2} e^{-2\beta_0 kd} \left[\frac{2J_1(Rq)}{Rq}\right]^2}_{I_{\text{Airy}}^{\text{spon}}(q)} \tag{6}$$

Here $I_{\text{Airy}}^{\text{spon}}(q)$ is the spontaneous pattern and $F_{\text{NL}}(q)$ is a non-linear q-dependent function given by,

$$F_{\text{NL}}(q) = \frac{1 - e^{-2kd(\beta_0 + \beta_{\text{NL}})}}{1 - e^{-2kd\beta_0}} \qquad (7)$$

It represents the decrease of the XAS contrast $1 - I_{\text{trans}}^0/I_0^0$ (see Eq. (**??**)) upon stimulation, with the spontaneous ($\beta_{\text{NL}} = 0$) value $F_{\text{NL}}(q) = 1$ decreasing to the stimulated ($\beta_{\text{NL}} = -\beta_0$) value $F_{\text{NL}}(q) = 0$. The decrease of absorption arises from the preferential exponential growth of the dominant intensity within the central Airy cone, defined by the momentum transfer $q < q_0$, where $q_0 = 1.22\pi R$ is the first node of the Airy pattern. Energy conservation then requires a counterintuitive *decrease* of all (out-of-beam) diffracted intensities at $q > q_0$. In short, the central Airy peak grows at the expense of the outer rings.

The intensity in the stimulated *magnetic* diffraction pattern in the region $q > q_0$ is given by,

$$I_{\text{mag}}^{\text{stim}}(\boldsymbol{q}) = F_{\text{NL}}(q)\, C_{\text{NL}}\, I_0^0\, \frac{A^2}{\lambda^2 z_0^2}\, e^{-2\beta_0 kd} \, |D_{\hat{m}_z}(\boldsymbol{q})|^2 \qquad (8)$$

Here

$$D_{\hat{m}_z}(\boldsymbol{q}) = \frac{1}{A} \int_A \hat{m}_z(x,y)\, e^{-i(q_x x + q_y y)} \, dx\, dy \qquad (9)$$

is the Fourier transform of the magnetization pattern described by the unit orientation function in different domains given by $\hat{m}_z(x,y) = \pm 1$. The non-linear information is contained in the first two terms in (**??**), with $F_{\text{NL}}(q)$ given by (**??**) and

$$C_{\text{NL}} = \cosh\left[2(\Delta\beta_0 + \Delta\beta_{\text{NL}})kd\right] - \cos\left[2(\Delta\delta_0 + \Delta\delta_{\text{NL}})kd\right] \qquad (10)$$

In the spontaneous limit we have $C_{\text{NL}} \to \cosh\left[2\Delta\beta_0 kd\right] - \cos\left[2\Delta\delta_0 kd\right]$, so that the intensity of the stimulated relative to the spontaneous magnetic diffraction pattern in the region $q > q_0$ is given by,

$$\frac{I_{\text{mag}}^{\text{stim}}}{I_{\text{mag}}^{\text{spon}}} = \frac{1 - e^{-2(\beta_0 + \beta_{\text{NL}})kd}}{1 - e^{-2\beta_0 kd}}$$
$$\times \frac{\cosh\left[2(\Delta\beta_0 + \Delta\beta_{\text{NL}})kd\right] - \cos\left[2(\Delta\delta_0 + \Delta\delta_{\text{NL}})kd\right]}{\cosh\left[2\Delta\beta_0 kd\right] - \cos\left[2\Delta\delta_0 kd\right]} \qquad (11)$$

Results for the calculated diffraction pattern, using the experimental geometry and a sample with a similar worm domain pattern, are shown in Fig. **??** (a) for two intensities differing by three orders of magnitude as in Fig. **??**. Both β_0^p and β_{NL}^p were calculated with the stated values of the parameters (same as in Table 1 of [**?**]), and convolution of the Lorentzian lineshape with a Gaussian of FWHM 1.4 eV to account for the band-structure broadening of the natural Lorentzian linewidth of 430 meV (see

Fig. 1 of [**?**]). In excellent agreement with the experiment results, the magnetic diffraction contrast is seen to be greatly diminished at the higher incident intensity of 270 mJ/cm^2/pulse and the Airy pattern is also less pronounced (see inner rings).
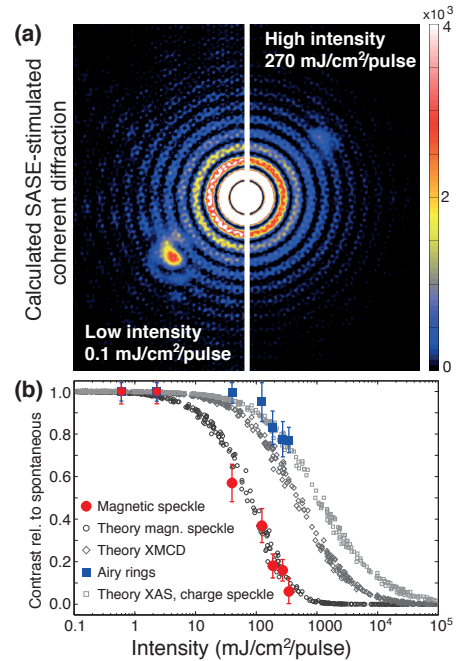

FIG. 4: (a) Calculated low intensity (left half) and high intensity (right half) diffraction patterns revealing the decrease of the contrast due to stimulated scattering. (b) Comparison of the observed magnetic (red) and Airy diffraction contrast (blue) and calculated change (gray) upon stimulation. The calculated XAS and XMCD intensities are the same as in Ref. [**?**] but include pulse-to-pulse statistical variations in coherence time and photon energy for a given total pulse intensity.

In Fig. **??** (b) we compare the experimental intensity-dependent magnetic (red circles) and Airy ring (blue squares) diffraction contrasts with our simulations shown in gray. The experimental contrasts were determined by analysis of radial diffraction intensity plots as shown in Fig. **??**. The red data points represent the magnetic diffraction contrast around $q = 0.03\,\text{nm}^{-1}$ relative to the spontaneous contrast recorded at low intensity, and the blue data points represent the relative "charge" contrast which is reflected by the intensity of the Airy rings for $q \geq 0.007\,\text{nm}^{-1}$.

The simulations included statistical variations in coherence time for a given pulse intensity [**?**], which is seen to be relatively small. The contrasts were calculated by means of Eqs. (**??**), (**??**) and (**??**) without any adjustment of the parameters given in Ref. [**?**]. This shows convincingly that the observed contrast reduction is indeed due to stimulated forward scattering.

The characteristic disappearance of *both* charge and magnetic contrast cannot be explained by ultrafast demagnetization during the 50 fs x-ray pulse itself. Demagnetization of Co/Pd after optical excitation has been observed on longer timescales >200 fs and it is typically limited to about 50% [?]. At our relatively low intensities, less than 1% of the atoms in the sample are in an excited state and we can also exclude multi-ionization as the reason for the contrast loss, as was previously suggested to occur at higher incident intensities [?].

Our results show that at an intensity of about $10 \, \mathrm{mJ/cm^2}$/pulse, the coherent incident field begins to control the temporal evolution of the electronic $2p_{3/2} \leftrightarrow 3d$ core-valence cycles, and stimulated decays begin to dominate over spontaneous Auger and radiative decays. Absorption and diffraction are progressively compensated by stimulated emission in the direction of the incident driving field. More generally, our results show that the control of nuclear spin transitions in the neV range utilized in nuclear magnetic resonance and the optical laser control of valence transitions in the eV range, can be extended to the control of atomic core-to-valence transitions in the keV range. The latter offer elemental, chemical, and magnetic specificity [?].

———————

* Electronic address: andreas.scherz@xfel.eu
† Electronic address: stohr@stanford.edu

[1] S. Eisebitt et al., Nature **432**, 885 (2004).
[2] H. N. Chapman et al., Nature Physics **2**, 839 (2006)
[3] M. J. Bogan et al., Nano Lett. **8**, 310 (2008).
[4] P. Tibault et al., Science **321**, 379 (2008).
[5] I. Robinson and R. Harder, Nature Materials **8**, 291 (2009).
[6] H. N. Chapman and K. A. Nugent, Nature Photonics **4**, 833 (2010).
[7] H. N. Chapman et al., Nature **470**, 73 (2011).
[8] M. M. Seibert et al., Nature **470**, 78 (2011).
[9] T. Wang et al., Phys. Rev. Lett. **108**, 267403 (2012).
[10] R. Neutze and R. Wouts and D. van der Spoel and E. Weckert and J. Hajdu, Nature, **406**, 752 (2000).
[11] C. Bostedt et al., Rev. Mod. Phys. **88**, 015007 (2016).
[12] L. Young et al., Nature, **466**, 56, (2010); J. P. Cryan et al., Phys. Rev. Lett. **105**, 083004 (2010); B. Nagler et al., Nature Phys. **5**, 693 (2009); G. Doumy et al., Phys. Rev. Lett. **106**, 083002 (2011);
[13] N. Rohringer et al., Nature **481**, 488 (2012); M. Beye et al., Nature **501**, 191 (2013); H. Yoneda et al., Nature **524**, 446 (2015).
[14] C. Weninger et al. Phys. Rev. Lett. **111**, 233902 (2013).
[15] J. Stöhr and A. Scherz, Phys. Rev. Lett. **115**, 107402 (2015); Erratum: Phys. Rev. Lett. **116**, 019902 (2016).
[16] O. Hellwig, J. B. Kortright, A. Berger and E. E. Fullerton, J. Magn. Magn. Mater. **319**, 13 (2007).
[17] W. F. Schlotter et al., Appl. Phys. Lett. **89**, 163112(2006).
[18] J. Stöhr and H. C. Siegmann, *Magnetism: From Fundamentals to Nanoscale Dynamics*, (Springer, 2006)
[19] J.P. Hannon, G.T. Trammell, M. Blume, D. Gibbs, Phys. Rev. Lett. **61**, 1245 (1988).
[20] E. L. Saldin, E. A. Schneidmiller, M. V. Yurkov, New J. Phys. **12** 035010 (2010).
[21] I. A. Vartanyants et al., Phys. Rev. Lett. **107**, 144801 (2011).
[22] A.A. Lutman et al., Phys. Rev. Spec. Topics - Accel. and Beams **15**, 030705 (2012).
[23] P. Heimann et al., Rev. Sci. Instrum. **82**, 093104 (2011).
[24] C. Boeglin et al., Nature **465**, 458, (2010). B. Vodungbo *et al.*, Nature Comm. **3**, 1, (2012).
[25] L. Müller et al., Phys. Rev. Lett. **110**, 234801 (2013).